Bio-Design and Manufacturing (2022) 5:674–686
https://doi.org/10.1007/s42242-022-00206-2

RESEARCH ARTICLE

Establishment of organoid models based on a nested array chip for fast and reproducible drug testing in colorectal cancer therapy

Yancheng Cui[2] · Rongrong Xiao[3] · Yushi Zhou[2] · Jianchuang Liu[3] · Yi Wang[3] · Xiaodong Yang[2] · Zhanlong Shen[2] · Bin Liang[2] · Kai Shen[2] · Yi Li[4] · Geng Xiong[4] · Yingjiang Ye[2] · Xiaoni Ai[1]

Received: 29 April 2022 / Accepted: 11 July 2022 / Published online: 6 September 2022

Abstract

The conventional microwell-based platform for construction of organoid models exhibits limitations in precision oncology applications because of low-speed growth and high variability. Here, we established organoid models on a nested array chip for fast and reproducible drug testing using 50% matrigel. First, we constructed mouse small intestinal and colonic organoid models. Compared with the conventional microwell-based platform, the mouse organoids on the chip showed accelerated growth and improved reproducibility due to the nested design of the chip. The design of the chip provides miniaturized and uniform shaping of the matrigel that allows the organoid to grow in a concentrated and controlled manner. Next, a patient-derived organoid (PDO) model from colorectal cancer tissues was successfully generated and characterized on the chip. Finally, the PDO models on the chip, from three patients, were implemented for high-throughput drug screening using nine treatment regimens. The drug sensitivity testing on the PDO models showed good quality control with a coefficient of variation under 10% and a Z' factor of more than 0.7. More importantly, the drug responses on the chip recapitulate the heterogeneous response of individual patients, as well as showing a potential correlation with clinical outcomes. Therefore, the organoid model coupled with the nested array chip platform provides a fast and reproducible means for predicting drug responses to accelerate precise oncology.

Graphic abstract

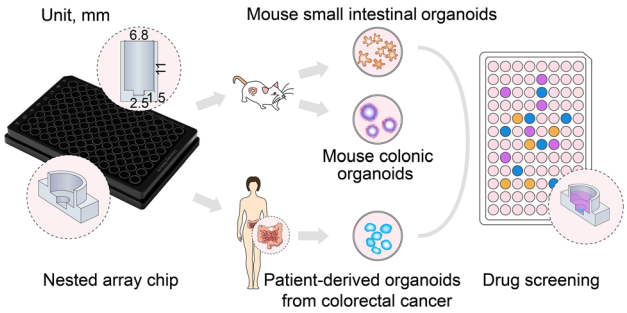

Keywords Organoid on chip · Patient-derived organoids · Precise oncology · Colorectal neoplasm · Drug screening

Yancheng Cui and Rongrong Xiao have contributed equally to this work.

✉ Yingjiang Ye
yeyingjiang@pkuph.edu.cn

✉ Xiaoni Ai
aixn@bjmu.edu.cn

[1] State Key Laboratory of Natural and Biomimetic Drugs, School of Pharmaceutical Sciences, Peking University, Beijing 100191, China

[2] Department of Gastrointestinal Surgery, Peking University People's Hospital, Beijing 100044, China

[3] Beijing Daxiang Biotech Co., Ltd., Beijing 100195, China

[4] Merck Innovation Hub (Guangdong) Co., Ltd., Guangzhou 510005, China

Introduction

Precise oncology refers to individual therapy tailored according to the predicted drug response, and aims to provide the most effective treatment for individual patients [1, 2]. Currently, next-generation sequencing (NGS) is widely used for clinical drug guidance by means of detecting drug target genes [3, 4]; however, very few patients benefit from it [5]. Another phenotypic model of patient-derived xenografts (PDXs) has been exploited to determine drug responses of patients [6, 7], but is time-consuming, high-cost, and has a low success rate and low throughput [8]. Recently, patient-derived organoids (PDOs) [9] have emerged as a reliable in vitro model with histological and genotypic characteristics highly similar to those of cancer tissues [8, 10]. Despite the progress made in the area of organoids, several technical bottlenecks still restrict their wide application. First, the relatively slow speed of organoid establishment restricts their applications in clinical practice [11]. Second, high variations in organoid size and drug response reduce the reproducibility and reliability of the results [8]. Usually, organoids are embedded in high concentrations of matrigel (≥50%, vol/vol) to maintain the essential components for organoid growth [12–15]. However, the difference in physical parameters and growth factor accessibility caused by high matrigel concentration induces variability in size and drug response of the organoids. Dr. Hans Clevers recommended using 5% matrigel for drug testing to improve reproducibility [16]. Some organoid cultures cannot survive in suspension, and comparison of screening results in different percentages of matrigel should be carried out with caution [16, 17]. Additionally, a low concentration of matrigel may alter the composition of secretion protein and organoid cell types, as well as drug response [18–20].

Integrating an organoid with a chip is a technique that may solve these technical challenges [21–23]. The chip can precisely control the microenvironment of organoids in terms of secretory factors, extracellular matrix, and cell–cell interactions [24, 25]. Recently, a hydrogel-based U-shaped microwell array chip was developed for suspension culture of organoids [18]. This technology provides a robust and reproducible organoid assay but in a matrigel-free manner. A PDO model has also been established on an integrated superhydrophobic microwell array chip [26]. This approach shortened drug-sensitivity testing time to one week. However, the nanoliter scale of the microwells on the chip promoted variability and heterogeneity of the organoids from well to well, thus necessitating baseline calibration before detection. Microfluidic-driven droplet chips and three-dimensional (3D) bioprinting offer promising platforms to speed up organoid assays and generate organoids with uniform size [11, 27, 28]. The fluid and temperature control equipment are operationally complex and expensive, however. To our knowledge, none of the organoid-on-chip models have met all the requirements for fast, high reproducibility and low cost with the use of high-concentration matrigel.

Here, we established organoid models on a nested array chip for fast and reproducible drug testing using 50% matrigel. First, we characterized mouse intestinal and colonic organoid models. The growth speed and robustness of the mouse organoid models cultured on the chip and microwell plate were compared. Next, we established a PDO model from colorectal cancer on the chip. The PDO model and parental tumor were compared in terms of histopathology, DNA copy number variations (CNVs), and mutation profiles. Finally, we carried out PDO-based drug sensitivity testing and analyzed its consistency with clinical outcomes from three patients. We envision organoid models on chips as a promising platform for screening the most effective treatment for cancer patients.

Materials and methods

Materials and reagents

See Tables 1, 2 and 3 below.

Table 1 Culture reagents

Name	Vendor	Cat#
Matrigel	Corning	356231
Cell Titer-Glo® 3D Cell Viability Assay	Promega	G9683
Ki-67 (D3B5) Rabbit mAb (Alexa Fluor® 488 conjugated)	CST	11882S
Rb mAb to EpCAM (Alexa Fluor® 647 conjugated)	Abcam	Ab23738
DAPI	Macgene	CD051
Ki-67 (8D5) Mouse mAb	CST	9449S
CDX2 (D11D10) Rabbit mAb	CST	12306S
CK20 (Keratin 20 (D9Z1Z) XP® Rabbit mAb)	CST	130663S

Table 2 Compound information

Name	Vendor	Cat#
5-Fluorouracil (5-FU)	MCE	HY-90006
Oxaliplatin	MCE	HY-17371
Irinotecan (CPT-11)	MCE	HY-16562
Regorafenib	MCE	HY-10331
Fruquintinib	MCE	HY-19912
Cetuximab	MCE	HY-P9905

Table 3 Experimental instruments

Name	Vendor	Model number
Confocal laser-scanning microscope	Nikon	Model eclipse Ts2
Microplate reader	BioTek	H1 M
Cellometer® Mini Cell Counter	Nexcelom	Mini-006–0783

Nested array chip plate

A nested array chip was used to establish the organoid models. We designed a nested array chip with AutoCAD software. The standard 96-microwell plate was used as a prototype to design the chip, which was 127.8 mm long, 85.5 mm wide, and 9 mm center-to-center. The chip consisted of 96 units that were compatible with high-throughput apparatus. Each unit had a nested design with a reservoir and a 3D implanting hole. The 3D implanting hole had a diameter of 2.5 mm and height of 1.5 mm, while the reservoir had a diameter of 6.8 mm and height of 11 mm. The reservoir and 3D implanting hole were made of polystyrene and manufactured by injection molding. The two layers of polystyrene were joined by biocompatible adhesive tape.

Construction of mouse organoid models on the chip and microwell plate

Mouse intestinal and colonic organoids were extracted from mice and expanded in the 60%–100% matrigel, as described previously [29–31]. The organoids were digested into single cells or clusters, and the number of cells/clusters was counted with the cell counter or microscopy. After that, the organoid suspension was centrifuged and resuspended in 50% matrigel to obtain the desired concentrations. To establish the mouse organoid model on the chip, an 8-μL mixture was seeded into the 3D implanting hole of the chip and then solidified at 37 °C for 10 min. The seeding number of the mouse intestinal organoids (10, 20, and 30 clusters per hole) and colonic organoids (50, 125, 250, and 500 cells per microliter) was different based on their growth speed. The seeding volume of the mouse intestinal organoids on the microwell plate was 8 or 20 μL of matrigel with the same organoid seeding number of 10, 20, and 30 clusters per hole. To construct the mouse colonic organoid model on the microwell plate, we also added 8 μL (250 cells per microliter) or 20 μL (100 cells per microliter) of the mixture into a 96-well plate. The mixture formed solidified domes containing the same number of cells (2000 cells per hole). 100 μL of complete organoid growth medium was added into the reservoirs of the chip and 96-well plate. The culture medium was composed of advanced DMEM/F12 (Gibco), 1% penicillin/streptomycin (Macgene), 10 mM HEPES (Gibco), 1% glutamax (Gibco), 1X N2 (Invitrogen), 1X B27 (Invitrogen), 1 mM *N*-acetylcysteine (Sigma), 10 mM nicotinamide (Sigma), 500 nM A-83-01 (Tocris), 3 μM SB202190 (Sigma), 10 nM prostaglandin E2 (Sigma), 10 nM gastrin I (Sigma), and 50% R-spondin3-Noggin-Wnt3a conditioned medium (L-WRN cell line, ATCC, CRL-3276). The organoids were imaged every 2–3 days during medium replacement. The organoid size and number of budding structures within the individual organoids were measured. The bright-field images of each group of the organoids were captured under the microscope with a 10× objective on three non-overlapping focal planes. The area of the organoids was analyzed with Image-Pro Plus 6.0 software.

Establishment of the patient-derived organoid (PDO) model on the chip

All tissue collection and experiments were reviewed and approved by the ethical committees of Peking University People's Hospital (Ethics approval number: 2021PHB148-001) and registered in ClinicalTrial.gov (NCT04996355). Patient pathological information was provided by the hospital, and all patients provided written informed consent to allow research use of the tissues.

Gastrointestinal cancer tumor tissues were washed five times with cold phosphate-buffered saline (PBS) supplemented with antibiotics, and then minced into fragments with a size smaller than 2 mm^3. The tissue fragments were chemically digested with 1 mg/mL collagenase A (Roche Diagnostics) at 37 °C for 10–15 min on an orbital shaker, and then mechanically dissociated by repetitive pipetting in the cold DMEM/F12 for 4–5 times. The supernatant was passed through a 70-μm cell strainer, centrifuged, and seeded into 100% matrigel in a 24-well tissue-culture plate. After polymerization for 10 min at 37 °C, the matrigel dome was overlaid with 500 μL of organoid culture medium. The culture medium was composed of advanced Dulbecco's modified Eagle medium/F12 supplemented with 1X B27, Glutamax, 10 mM HEPES (Gibco), 100 μg/mL primocin (InvivoGen), 50 ng/mL recombinant human EGF (Peprotech), 10 nM gastrin (Sigma), 500 nM A83-01 (Tocris Bioscience), 1.25 mM *N*-acetylcysteine (Sigma), 10 mM nicotinamide (Sigma), 100 ng/mL recombinant human Noggin (Peprotech)/10% Noggin conditioned media, and 20% R-spondin1 conditioned media. 10 μM Y-27632 dihydrochloride kinase inhibitor (Tocris Bioscience) was also added to the culture medium for 2–3 days. To establish the PDO model on the chip, 8 μL of 50% matrigel containing 1000 single cells was seeded into the 3D implanting hole of the chip, and then solidified at 37 °C for 10 min.

Immunofluorescence

Immunofluorescence images of the mouse organoids were captured directly on the chip. After being cultured for 7 days, the organoids were fixed with 4% paraformaldehyde in PBS for 30 min, and washed two times with PBS. Next, the organoids were permeabilized with Triton-X 100 in PBS for 30 min at room temperature. After blocking for 60 min in 3% bovine serum albumin (BSA) in PBS, the organoids were incubated with florescence-labelled primary antibodies (1:200) overnight at 4 °C. The organoids were washed with PBS and stained with 4′6-diamidino-2-phenylindole (DAPI) for nucleus visualization and finally imaged with a confocal microscope (Nikon).

Viability assessment of the organoids

The viability of the organoids was measured using CellTiter-Glo 3D cell viability assay (Promega) according to the manufacturer's instructions. Briefly, the CellTiter-Glo reagent and organoid culture medium were mixed with a volume ratio of 1:1. Luminescence was detected on a multiplate reader.

Hematoxylin and eosin (H&E) and immunohistochemistry staining

The PDOs were firstly recovered from matrigel with cell recovery solution (Corning). The PDOs and parental tissues were fixed with 4% freshly prepared paraformaldehyde at 4 °C for 24 h, dehydrated and embedded in paraffin blocks, and then cut into 5-μm slices. We carried out standard H&E and immunohistochemistry staining on these sections. For H&E staining, the sections were stained with hematoxylin and eosin. For immunohistochemistry staining, they were stained with primary antibodies of Ki-67, CDX2, and CK20, as mentioned above. H&E and immunohistochemical images were acquired by inverted microscopy (Olympus).

Whole-exome sequencing (WES) analysis

We harvested the PDOs and extracted their DNA. The samples were sent to Genetron Health (Beijing) Co., Ltd., where the staff of Genetron Health carried out WGS analysis with Illumina HiSeq. Sequence reads were aligned to the human reference genome GRCh37 using the Burrows–Wheeler alignment with maximal exact matches (BWA-MEM) (v0.7.10). Then BAM files were processed in terms of duplicate reads. Somatic variants were identified by providing the reference and tumor or organoid sequencing data to MuTect (v3.1-0-g72492bb) with default parameters. Effect predictions and annotations were added using ANNOVAR. To detect somatic CNAs, BAM files were analyzed for read-depth variations using Control-FREEC (V9.1), by comparing tumors or organoids to paracancerous tissue. Mutational signatures were analyzed using an R package called BSgenome.

The PDO models on the chip for drug screening

The PDO models were constructed on the chip for 3 days. Next, the drugs were administered to the models for 5 days. The drug panel was composed of nine regimens, including 5-FU, oxaliplatin, CPT-11, 5-FU + oxaliplatin (1:1), 5-FU + CPT-11 (1:1), 5-FU + oxaliplatin + CPT-11 (1:1:1), cetuximab, fruquintinib, and regorafenib. The highest concentration for each drug was 30 μM, except for cetuximab, which was 50 μM. A serial 1:3 dilution was performed with 9 serial dilutions with each vehicle. Dose–response curves and IC_{50} values were generated by cell viability against drug concentrations. The viability of the organoids was assessed as described, and the inhibition rate of cell viability was calculated according to the following formula:

$$\text{Inhibition rate}\,(\%) = \left(1 - \frac{\text{Fluorescence enhancement with drug administration}}{\text{Fluorescence enhancement without drug administration}}\right) \times 100.$$

Statistics

All the experiments were repeated at least three times. All the data were statistically analyzed with GraphPad Prism 9.0 software (San Diego, CA, USA). Quantitative data were plotted as the mean ± standard error. Statistical analysis was performed using two-way analysis of variance (ANOVA). Differences were indicated to be significant when $^{*}p<0.05$, $^{***}p<0.001$.

Results

Superior performance of mouse organoid models on the chip

Organoid models from mice and human beings were established on the array chip using 50% matrigel (Fig. 1a). The chip consisted of 96 units that were compatible with high-throughput equipment, such as a liquid dispenser, multichannel liquid handler, and micro-plate reader. The chip had a reservoir layer on the top, a 3D implanting hole in the middle, and a glass slide underneath. The nested design allowed convenient medium exchange without disruption of the 3D organoids. The open-top design also allowed easy access for changing the culture medium and for drug administration. The bottom of the chip was ultra-thin transparent optical glass, which was compatible with confocal microscopes and

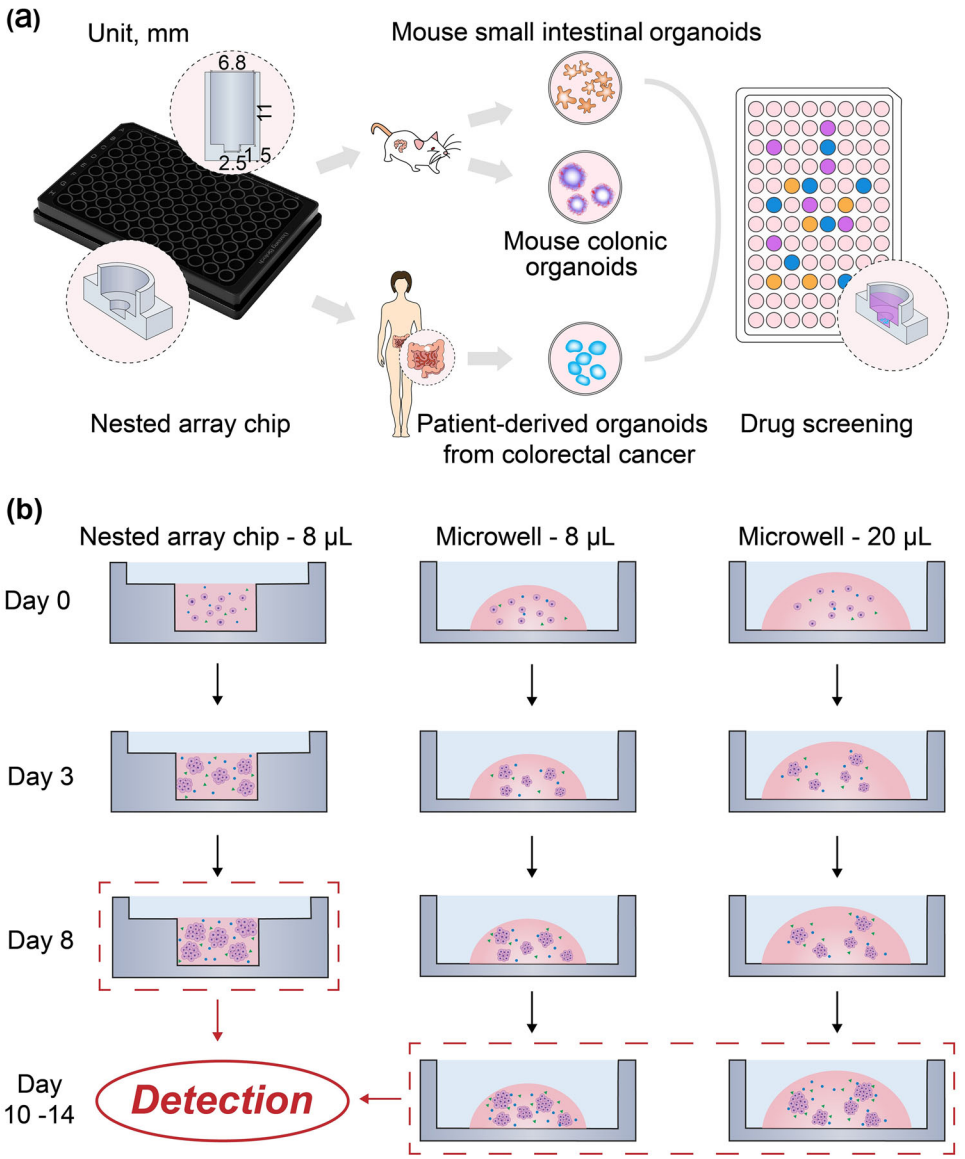

Fig. 1 Schematic showing establishment of organoid models on a nested array chip for drug screening and detection of growth kinetics of the organoids among different culture platforms. **a** Schematic showing chip design, establishment of organoid models, and on-chip drug screening. A magnified sketch showing the cross-section of one unit of the chip. A 3D implanting hole was used for seeding the mixture of matrigel (50%, vol/vol) and organoids. The drugs were added into the reservoir. **b** Schematic of the growth kinetics of the organoids on different culture platforms on different days

high-content imaging devices for high-quality imaging. It also had a unique anti-evaporation design to prevent the edge effect. This chip is also suitable for 3D cell culture based on various types of hydrogels that provide a more biomimetic microenvironment with cell and extracellular matrix interaction [32]. The established organoid models on the array chip were used for high-throughput drug screening. We established three methods for organoid culture, including 8 μL of matrigel on the nested array chip, 8 μL of matrigel on the microwell plate, and 20 μL of matrigel on the microwell plate (Fig. 1b). The idea behind this was that different culture platforms might affect organoid growth kinetics and variability.

Firstly, the mouse small intestinal and colonic organoids were successfully established on the chip. The size of the organoids on the chip increased over 5 days of culture, and displayed a classic small intestinal morphology (Figs. S1 and S2 in Supplementary Information). The use of ultra-thin glass on the underside of the chip allowed the mouse organoids to be characterized in situ by confocal imaging. As shown in Fig. 2a, these organoids consisted of an inner lumen surrounded by the crypt and villus domains (Fig. 2a, left). They displayed various cell types, including mature epithelial cells and proliferating intestinal progenitor cells, as previously reported [32]. The mouse colonic organoids also showed a specific morphology with a circular lumen, but no obvious budding structures (Fig. 2a, right).

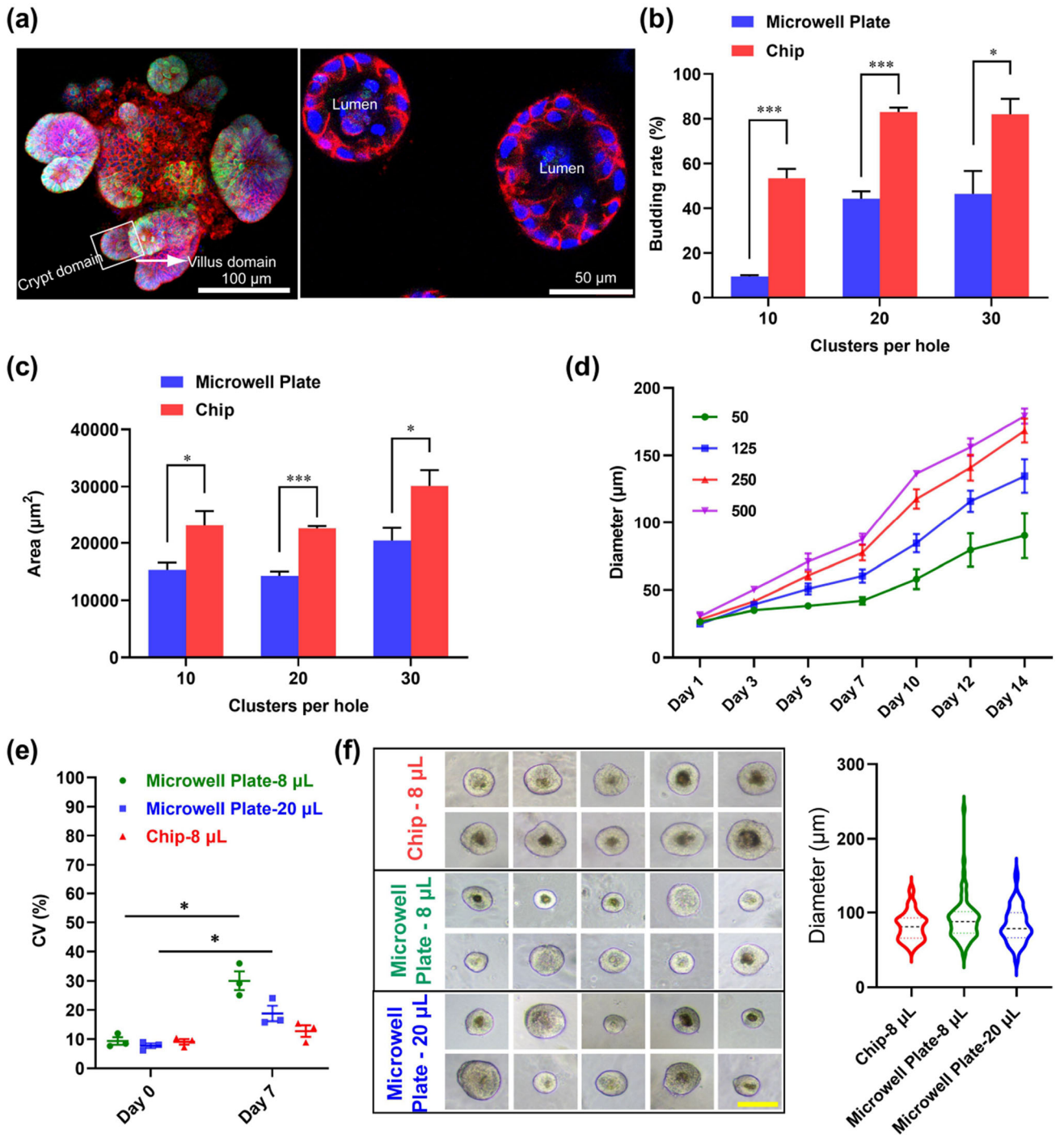

Fig. 2 Superior performance of mouse organoid models cultured on the chip. **a** Confocal image of immunofluorescence staining of the mouse small intestinal organoids (left) and colonic organoids (right) on day 7. Mature epithelial cells labeled in red with Alexa Fluor® 647-conjugated EpCAM antibody, proliferating intestinal progenitor cells labeled in green with Alexa Fluor® 488-conjugated Ki-67 antibody, and nuclei stained in blue with DAPI. **b**, **c** Comparison of the budding rate (**b**) and growth area (**c**) of the mouse intestinal organoids between those on the chip and those in the 96-microwell plate. The seeding volume of mouse intestinal organoids was 20 μL of matrigel on the microwell plate, but 8 μL of matrigel on the chip. **d** Growth curve of the mouse colonic organoids with different seeding densities (cells per microliter) on the chip. **e** Comparison of the CV values of the colonic organoids in ATP activity among the three platforms. The seeding number of the organoids on all three platforms was consistent with 2000 cells per hole. $^{*}p<0.05$, $^{***}p<0.001$. **f** Bright-field images showing the representative organoid size and violin plot showing the frequency distribution of organoid size on different culture platforms on day 7. Scale bar, 100 μm

We also compared the growth speed of the mouse organoid models on the chip and in the conventional microwell plate. The same numbers of mouse small intestinal organoids (10, 20, or 30 organoids per hole) were first seeded onto the two platforms with different seeding densities. Compared with the conventional microwell plate with 20 μL matrigel, the organoids cultured on the chip with 8 μL of matrigel showed an enhanced budding rate and larger growth area (Figs. 2b and 2c). The budding rate and growth area of the small intestinal organoids also increased with the initial organoid seeding number of clusters on the two platforms. This result was further validated with the mouse colonic organoids cultured on the chip. The higher seeding density induced faster growth of the colonic organoids (Fig. 2d). A previous report indicated that organoid growth was dependent on secretory factors [33]. The higher density of organoids on the chip may slow down diffusion of secretory factors, as well as enhance cell–cell communication in a more physiological way. These results indicated that the chip platform promoted organoid growth when seeding density was increased because of cumulative concentrations of secretory factors.

Finally, we compared the robustness of the mouse organoid models between the chip and the conventional microwell plate. The coefficient of variation (CV) of ATP activity in the mouse intestinal organoids was much smaller on the chip (Fig. S3 in Supplementary Information). With increased culture time, the CV values of size in mouse colonic organoids were also below 15% (Fig. S4 in Supplementary Information). To further explore why the chip platform achieved higher reproducibility, we quantitated CV values of the mouse colonic organoids among the three platforms (Fig. 2e). The CV values of the organoids on seeding day (day 0) showed no significant difference among the three groups. However, the lowest CV value of approximately 12% was achieved on the chip on day 7. The microwell plate showed the highest CV value of approximately 30% with the same seeding volume of matrigel as other platforms. The representative organoid size of the three culture platforms on day 7 also illustrated that the organoid culture on the chip displayed less variability (Fig. 2f). These results indicated that the chip with the nested design could provide a precisely controlled microenvironment for the organoid culture. Compared with the dome shape of the matrigel on the microwell plate, the implanting hole on the chip restricted the matrigel in the fixed location and cylinder shape. The physical parameters and growth-factor accessibility of all the organoids on the chip were highly similar. The nested design of the chip also allowed convenient medium exchange without disruption of the 3D organoids. Therefore, the high reproducibility of the organoids on the chip may be due to the uniform shaping of the matrigel and gentle medium exchange.

Taken together, the chip platform promoted organoid growth and improved reproducibility by its nested design.

Establishment and characterization of the PDO model on the chip

To further explore the capability of the chip platform for precise oncology, we constructed a PDO model derived from colorectal tumors. The implanting hole on the chip was seeded with a mixture of 8 μL matrigel and 1000 single cells. The size of the organoids on the chip increased over time and achieved a diameter of 100 μm within 7 days (Fig. 3a). We created a violin plot showing the frequency distribution of PDO size on the chip on day 7 (see Fig. S5 in Supplementary Information). Therefore, the drug screening regimen on the PDO model could be carried out within one week. Consistent with a previous study [34], Hematoxylin and eosin (H&E) staining showed that the PDOs on the chip presented heterogeneous morphologies with predominantly thin-walled cystic structure (Patient 1) and solid dense structure (Patient 3) (Fig. 3b). Immunohistochemistry staining further showed that all the PDO models expressed colorectal tumor specific markers of CDX2, CK20, and Ki-67. Moreover, the PDO model on the chip resembled the histological characteristics of the corresponding tissues. Next, we assessed whether the PDO model maintained genomic profiles of the parental tumors. Genome-wide CNV analysis showed that DNA copy-number losses and gains of the parental tumors were retained within the organoids (Fig. 3c). The point mutation type of the corresponding tissues was also conserved in the organoids (Fig. 3d). Moreover, the PDO model on the chip mostly recapitulated the profile of CNV cancer driver genes (Fig. 3e). Overall, our results demonstrated that the PDO model on the chip preserved the major characteristics of the parental tumor tissues.

The PDO models on the chip for reproducible drug screening

To explore the utility of the PDO model for precise oncology, the PDO models from three patients were established on the chip for drug-sensitivity screening. A drug panel was composed of drugs commonly used in clinical practice for colorectal cancer, including three chemotherapeutic drugs, three targeted drugs, and three chemotherapeutic combinations. The chemotherapeutic drugs were single agents from the chemotherapeutic combinations of Folfox (5-FU + oxaliplatin), Folfiri/Xeliri (5-FU + CPT-11), and Folfoxiri (5-FU + oxaliplatin + CPT-11). The targeted drugs were cetuximab, fruquintinib, and regorafenib. The dose–response curves and IC_{50} values were generated based on viability against drug concentration with nine serial dilutions (Figs. 4a–4i, S6, and S7). The IC_{50} values of the drugs displayed inter-patient heterogeneity (Fig. 4j). We ranked drug efficacy in sequence according to IC_{50} values. For example, the PDO models from patients 1 and 3, but not patient 2, showed sensitivity

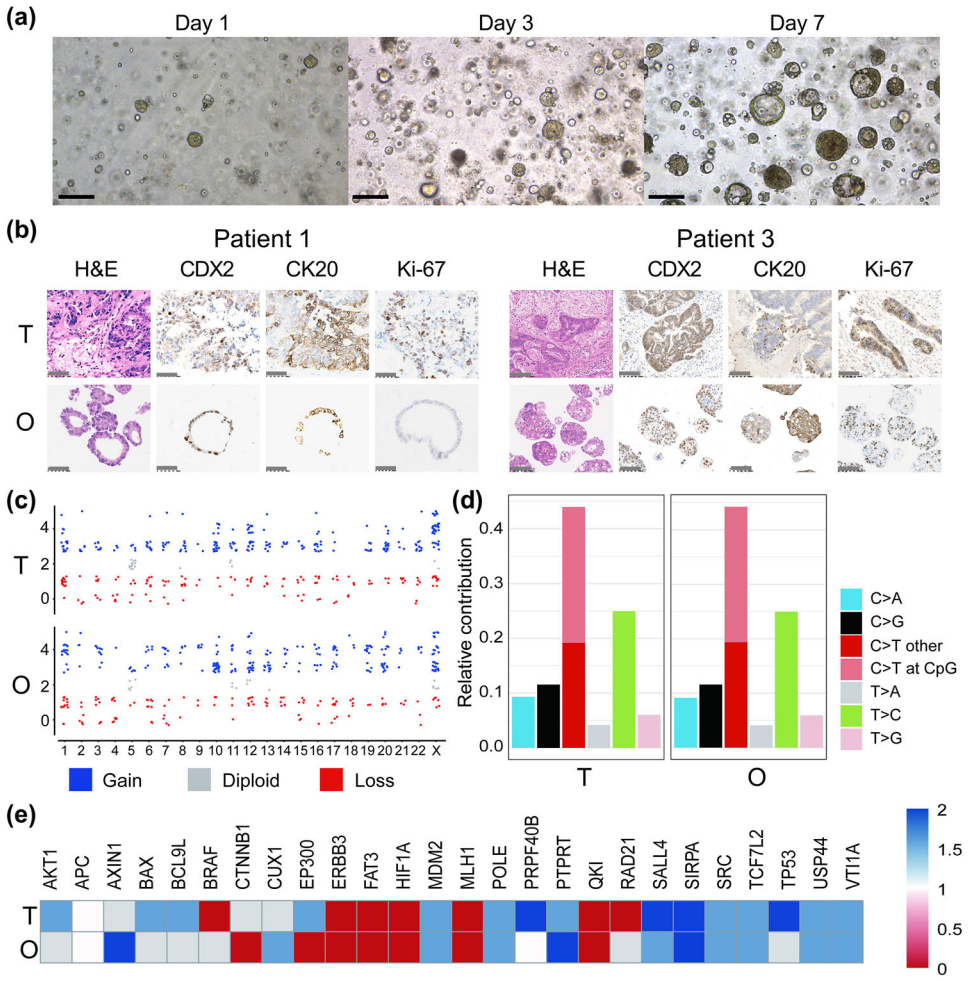

Fig. 3 Characterization of the PDO model on the chip. **a** Bright-field images of the PDOs over time on the chip. Scale bar, 100 μm. **b** H&E and immunohistochemical staining images of the PDOs (O) and parental tumors (T). Comparison of colorectal cancer markers (CDX2 and CK20) and a proliferation marker (Ki-67). Scale bar, 50 μm. **c** Genome-wide gene CNVs of the PDOs and parental tumors (blue, gains; gray, diploid; red, losses). **d** Bar graphs displaying frequency of point mutation types in the PDOs and paired tumor. **e** Heatmap of CNVs in cancer driver genes. Gene copy numbers are transformed as log2 ratios per gene (blue, gains; red, losses)

to oxaliplatin. It is known that regorafenib and fruquintinib are small-molecule anti-VEGF agents. However, patient 2 exhibited more sensitivity to regorafenib but not to fruquintinib, indicating that the multikinase inhibitor of regorafenib is effective on both tumor cells and vascular endothelial cells [34]. Moreover, all the PDO models on the chip were resistant to cetuximab due to the lack of EGFR-activating mutations. Additionally, the PDO models on the chip achieved high screen quality with an average CV of under 10% and Z' factor of approximately 0.75 (Figs. 4k and 4l). Therefore, the PDO models on the chip provided a reproducible platform for drug screening, as well as recapitulating the heterogeneous response of individual patients to anticancer drugs.

Drug-sensitivity testing of the PDO model on the chip predicted clinical outcomes of patients undergoing chemotherapy

Lastly, we evaluated whether the PDO model on the chip could predict clinical drug responses by using three patients as case studies. The overall diagnosis and drug treatment procedures of patient 1 are summarized in Fig. 5a. The patient was a 71-year-old woman who first underwent radical resection of a rectal tumor leading to a postoperative pathological stage of T4N1M0. A six-cycle Folfox regimen (5-FU 150.0 mg + oxaliplatin 4.25 g) was then performed. Recurrence of the anastomosis was generated in the 37th month, as evidenced by the enhanced CT scan of the chest, abdomen, and pelvis. Colonoscopy and pathology also confirmed moderately differentiated adenocarcinoma. The previous Folfox chemotherapy was considered to be sensitive because the recurrence of anastomosis generally occurred within two years after the radical surgery. The patient then underwent salvage enlarged sigmoid colon resection and a double hysterectomy. Intraoperative and postoperative pathology confirmed that the intestinal tissue, left ovary, and fallopian tube showed moderately differentiated adenocarcinoma infiltration. During the second surgery, we constructed the PDO model on the chip for drug sensitivity testing. The PDO model showed positive responses to both the Folfox (5-FU

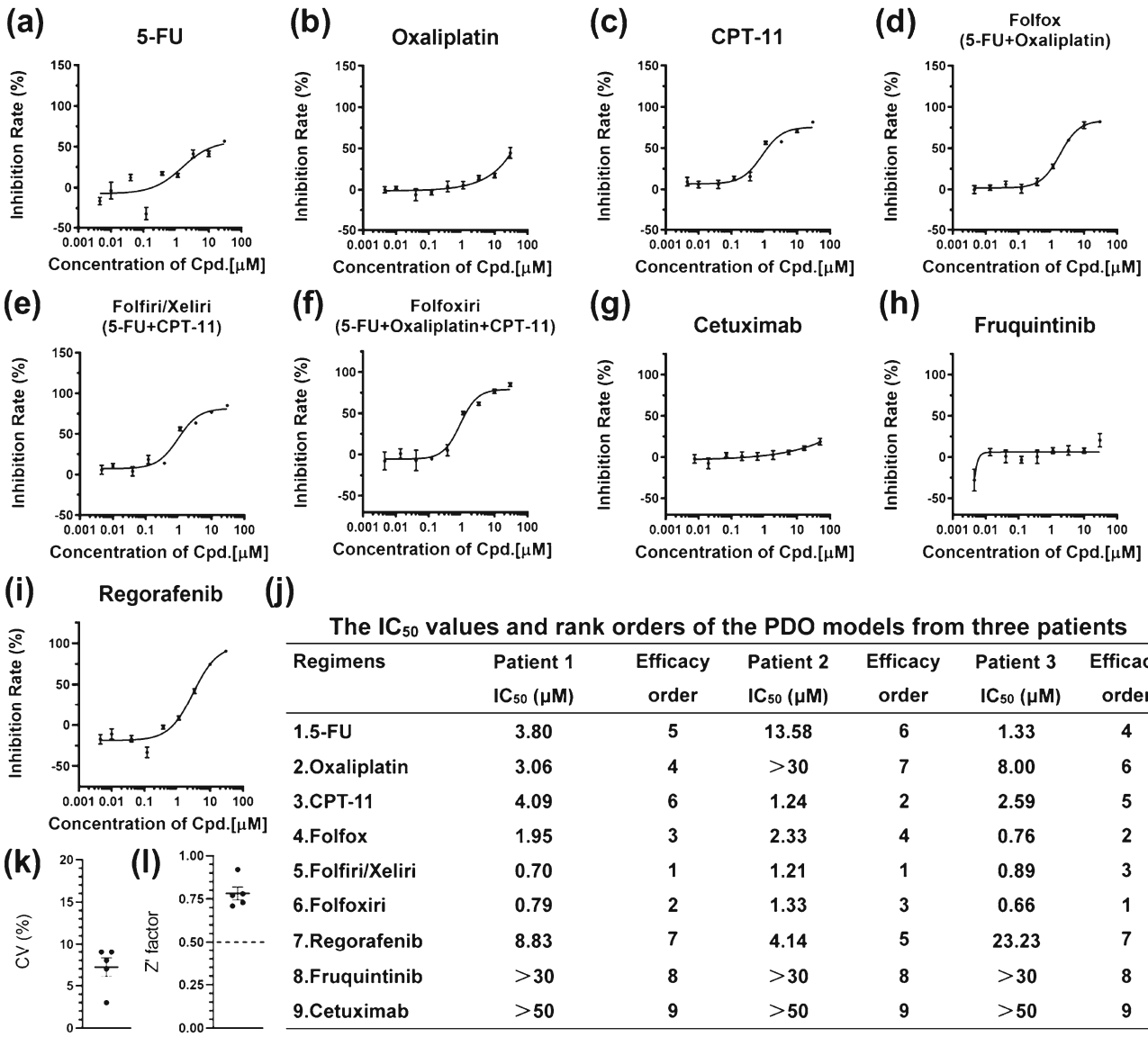

(j) The IC_{50} values and rank orders of the PDO models from three patients

Regimens	Patient 1 IC_{50} (μM)	Efficacy order	Patient 2 IC_{50} (μM)	Efficacy order	Patient 3 IC_{50} (μM)	Efficacy order
1.5-FU	3.80	5	13.58	6	1.33	4
2.Oxaliplatin	3.06	4	>30	7	8.00	6
3.CPT-11	4.09	6	1.24	2	2.59	5
4.Folfox	1.95	3	2.33	4	0.76	2
5.Folfiri/Xeliri	0.70	1	1.21	1	0.89	3
6.Folfoxiri	0.79	2	1.33	3	0.66	1
7.Regorafenib	8.83	7	4.14	5	23.23	7
8.Fruquintinib	>30	8	>30	8	>30	8
9.Cetuximab	>50	9	>50	9	>50	9

Fig. 4 Drug-sensitivity screening of the PDO models on the chip. **a–i** Dose–response curves of the nine chemotherapeutic regimens on the PDO model from patient 2, including 5-FU (**a**), oxaliplatin (**b**), CPT-11 (**c**), Folfox (5-FU + oxaliplatin) (**d**), Folfiri/Xeliri (5-FU + CPT-11) (**e**), Folfoxiri (5-FU + oxaliplatin + CPT-11) (**f**), cetuximab (**g**), fruquintinib (**h**), and regorafenib (**i**) (n=4). **j** Table showing the IC_{50} values and rank orders of the nine regimens from three PDO models on the chip. **k, l** CV value (**k**) and Z' factor (**l**) of the drug screening (n=5)

+ oxaliplatin) and Xeliri (5-FU + CPT-11) chemotherapies (Fig. 5b). Compared with Folfox, the Xeliri regimen exhibited more sensitivity, with a lower IC_{50} value of 0.70 μM. The patient unfortunately experienced recurrence of a vaginal stump tumor in the 39th month. The patient continued to undergo treatment with the Xeliri regimen (capecitabine 1500 mg bid po d2-d15 q3w + CPT-11 300 mg iv d1 q3w) for three cycles according to clinical practice. At the 42nd month, the enhanced CT scan showed that the tumor was significantly reduced, indicating that the Xeliri regimen was effective. This clinical outcome was consistent with the results from the PDO sensitivity testing on the chip.

Patient 2 was a 65-year-old male who was diagnosed with rectal cancer and liver metastases (Fig. 5c). He underwent a palliative resection due to complete bowel obstruction. The postoperative pathological stage was a moderately differentiated adenocarcinoma of the rectum (pT3N2bM1). The PDO model on the chip was established from the patient before post-operative Folfox chemotherapy. To mitigate the contamination issue that often occurs in bowel obstruction tissue [35], we quickly collected the tissue and repeatedly

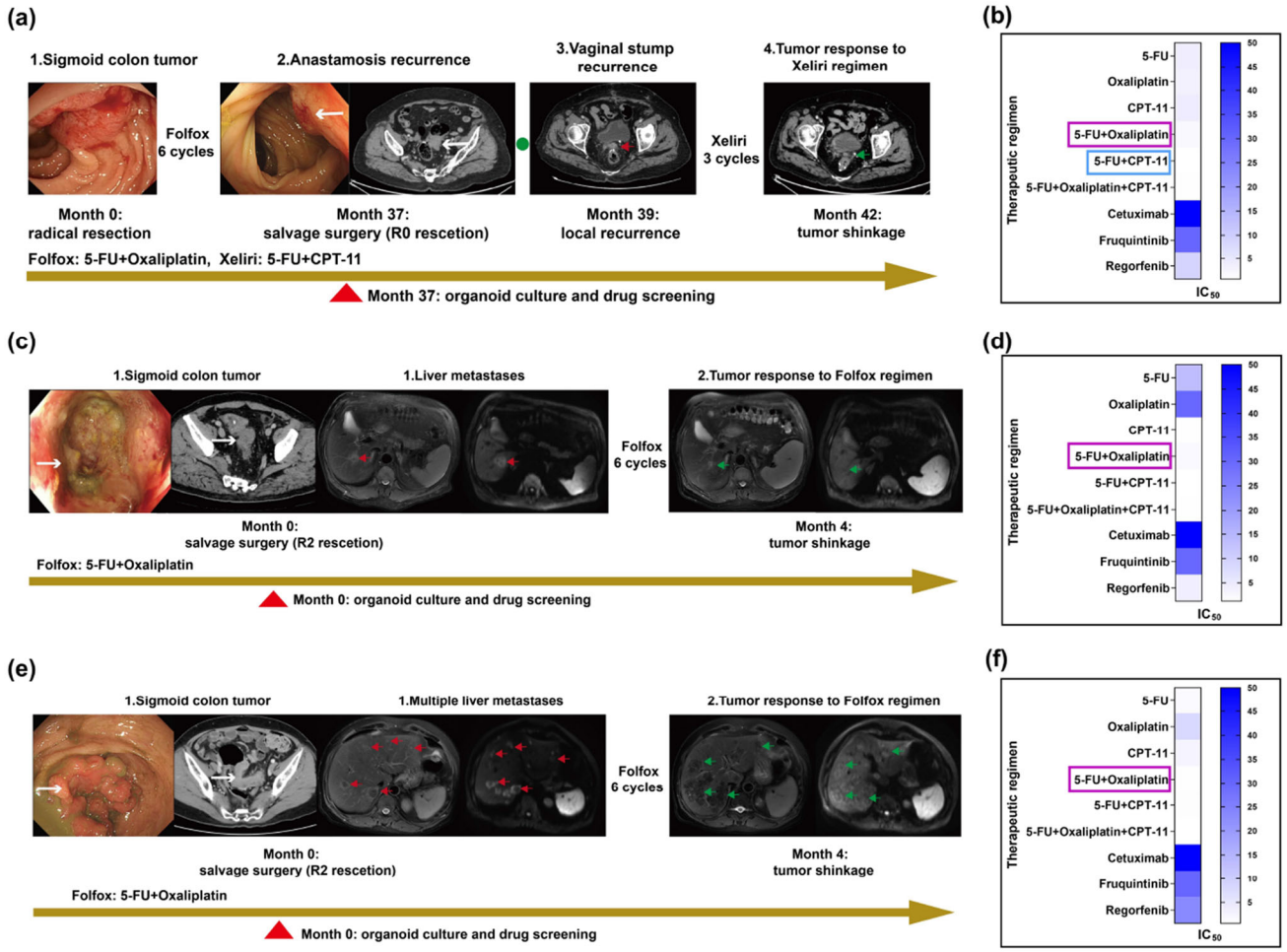

Fig. 5 PDO models on the chip predict clinical outcomes of three patients in response to chemotherapy. **a**, **c**, and **e** Timelines of diagnosis and drug treatment procedures for three patients, including patient 1 (**a**), patient 2 (**c**), and patient 3 (**e**). The white arrow indicates the primary/recurrent sigmoid colon tumor diagnosed by endoscopy and/or enhanced CT scan. The red and green arrows indicate the tumors before and after treatment with the chemotherapies, as indicated by enhanced CT scan and/or MRI scan. **b**, **d**, and **f** Heatmaps showing the IC_{50} values of the nine regimens in three PDO models, including patient 1 (**b**), patient 2 (**d**), and patient 3 (**f**). Clinically used chemotherapies are labeled in boxes

washed it before PDO-model establishment. Drug screening results showed that the Folfox regimen (5-FU + oxaliplatin) was sensitive (Fig. 5d). Indeed, the patient underwent Folfox chemotherapy for six cycles and the liver metastases were significantly reduced, as evidenced by magnetic resonance imaging (MRI). The clinical results indicated that the PDO model on the chip predicted the drug response for patient 2.

Patient 3 was a 66-year-old female with acute intestinal obstruction (Fig. 5e). An enhanced CT scan of the abdomen showed sigmoid cancer and liver metastases. Colonoscopy revealed a necrotic mass of the sigmoid colon 20 cm from the anal verge. MRI showed multiple foci of high metabolism in the liver. A six-cycle Folfox chemotherapy regimen was performed, with a positive response. The PDO model on the chip also showed sensitivity to the Folfox regimen (5-FU + oxaliplatin) (Fig. 5f). The clinical outcome was again in line with the PDO prediction.

Overall, these results indicated that the PDO models on the chip showed potential to predict the clinical outcomes of patients receiving chemotherapy.

Discussion

Tumor organoids are an in vitro biomimetic model to better study human development and diseases [36]. They conserve genetic heterogeneity of the tissue and recapitulate the cell microenvironment. However, establishment of these models is time-consuming and expensive. Organoid culture condition varies in laboratories, which inevitably leads to low

reproducibility of the research results [37]. Organoids on chips may offer an engineering approach to speed up and standardize organoid culture. Herein, we have established organoid models on a nested array chip for fast and reproducible drug testing in colorectal cancer therapy.

The organoid model established on the chip shows advantages over conventional methodology. First, our chip model accelerates the timeline of organoid development. The 3D implanting hole on the chip increases organoid seeding density and promotes growth of the organoids by increasing concentrations of secretory factors. Second, the model achieves high reproducibility of organoid size, cellular activity, and drug response. The 3D implanting hole on the chip provides uniform and controlled shaping of the matrigel that allows organoids to grow in a fixed location [38]. Additionally, consistency of organoid implantation is required between holes, which poses a challenge to matrigel-based organoid culture systems due to perturbation during replacement with fresh media [16]. The nested design of the chip allows convenient medium exchange without disruption of the 3D organoids. Third, the chip-based models are low-cost and operationally simple, which is especially critical for tissue samples with low volume. The miniaturized design of the implanting hole reduces organoid and matrigel consumption. Matrigel hydrogel has been widely used for organoid culture due to its close resemblance to the in vivo microenvironment. Sato et al. first grew murine intestinal Lgr5+ stem cells in high concentrations of matrigel [39–41]. Organoids can also be grown in other naturally derived proteins [40]. Previously, we used collagen materials to construct a 3D primary human hepatocyte model [20]. However, the collagen-based organoid culture changed organoid morphology [41]. Fourth, our model predicts heterogeneous responses of patients to chemotherapies in clinical settings. In clinical practice, it is still difficult for physicians to choose the drug with the best benefit for individuals. Clinical guidelines often recommend first-line homogenous treatment. However, it is inevitable that some patients will not benefit from it because of tumor heterogeneity. In this study, none of the three patients had oncogenic driver mutations. Therefore, the PDO models showed more sensitivity to the chemotherapeutic drugs than the targeted drugs. For example, none of the PDO models responded to the cetuximab targeting EGFR mutations. In addition, none of the patients responded to fruquintinib, which is a small-molecule inhibitor of VEGFR-1, -2, and -3 tyrosine kinase [42]. This result is due to lack of microvasculature on the PDO models. Interestingly, patient 2 exhibited sensitivity to regorafenib. We speculate that regorafenib inhibited receptor tyrosine kinases expressed on the tumor cells. It should be noted that a prospective study of the correlation of the PDO models and clinical outcomes with more patient cases is required.

The success of precision oncology relies on models that recapitulate the tumor microenvironment and predicate drug response for individual patients [43]. Organoids are a reliable in vitro model with high similarity to tissues, and offer an unprecedented opportunity for precise oncology. Recent studies have demonstrated that the sensitivity of PDO treated with chemotherapies is correlated to clinical outcomes [44]. Despite the progress made with organoids for precision oncology, the conventional microwell-based platform for organoid assays has drawbacks in terms of low speed, high cost, and high variation. In current clinical practice, the time between a diagnosis of cancer and the start of drug treatment ranges between 12 and 14 days [45]. Our methodology could obtain at least 324 independent data points within 14 days, which would meet the needs of timeliness for clinical practice and provide high-throughput drug screening for precise oncology. In addition, the cost of organoid culture for clinical usage is largely determined by materials such as the matrigel and culture medium. We established our organoid models on a miniaturized chip which reduces the cost by more than 50% compared with a conventional microwell plate. Furthermore, standardization of organoid culture is critical for bringing PDO technology to market. The PDO models on our chip exhibited a CV of under 10% and a Z' factor of approximately 0.75, which was superior to the conventional microwell plate (with a CV >20% and Z' factor >0.4). We believe automated approaches to establishing organoids are the most promising road to clinical implementation of PDOs.

Conclusions

We constructed organoid models on a nested array chip, which precisely controlled the microenvironment of the models. Compared with a conventional microwell-based platform, the chip sped up organoid growth, reduced organoid and matrigel consumption, and dramatically reduced variation in size and cellular activity. The patient-derived organoid (PDO) model on the chip also preserved morphology, protein markers, and gene expression of the parental tumors. More importantly, the PDO model on the chip reflected the heterogeneous response of individual patients to anti-tumor drugs, and showed the potential to predict the clinical outcome. As a standardized platform, the nested array chip allows for cell seeding and compound administration using robotic platforms for high-throughput screening. We are currently expanding our pilot trial from three patients to thirty to evaluate the consistency between the drug response of the PDO model on the chip and the clinical outcome of patients. We believe the model to be a promising tool to predict cancer patient outcomes.

Supplementary Information The online version contains supplementary material available at https://doi.org/10.1007/s42242-022-00206-2.

Acknowledgements This work was supported by grants from the National Natural Science Foundation of China (No. 82174086), the Beijing Natural Science Foundation (No. 7222273), the Beijing Xisike Clinical Oncology Research Foundation (Nos. Y-xsk2021-0004 and Y-XD202001-0172), the Youth Talents Promotion Project of China Association of Chinese Medicine (No. 2020-QNRC2-08), the Clinical Medicine Plus X-Young Scholars Project of Peking University (No. BMU2021MX009), and the Peking University People's Hospital Research and Development Funds (No. RDY2020-18).

Author contributions XA, YC, and RX contributed to conceptualization; XA, YC, RX, JL, YL, and GX provided methodology; XA, YC, RX, YZ, XY, ZS, BL, and KS provided resources; XA, YC, RX, and YW carried out data analysis; XA, YC, and YW performed writing—original draft preparation; XA performed writing—review and editing; XA and YY performed supervision; YC, XA, and YY contributed to funding acquisition. All authors have read and agreed to the published version of the manuscript.

Declarations

Conflict of interest XA is the scientific advisor at Beijing Daxiang Biotech. RX, JL and YW are current employees at Beijing Daxiang Biotech. YL and GX are current employees in Merck Innovation Hub (Guangdong) Co., Ltd..

Ethical approval The study was conducted in accordance with the Declaration of Helsinki and approved by the ethical committees of Peking University People's Hospital (Ethics approval number: 2021PHB148-001) and registered in ClinicalTrial.gov (NCT04996355). Informed consent was obtained from all patients for being included in the study.

References

1. Chae YK, Pan AP, Davis AA et al (2017) Path toward precision oncology: review of targeted therapy studies and tools to aid in defining "actionability" of a molecular lesion and patient management support. Mol Cancer Ther 16(12):2645–2655. https://doi.org/10.1158/1535-7163.Mct-17-0597
2. Tran A, Klossner Q, Crain T et al (2020) Shifting, overlapping and expanding use of "precision oncology" terminology: a retrospective literature analysis. BMJ Open 10(6):e036357. https://doi.org/10.1136/bmjopen-2019-036357
3. Mosele F, Remon J, Mateo J et al (2020) Recommendations for the use of next-generation sequencing (NGS) for patients with metastatic cancers: a report from the ESMO precision medicine working group. Ann Oncol 31(11):1491–1505. https://doi.org/10.1016/j.annonc.2020.07.014
4. Gulilat M, Lamb T, Teft WA et al (2019) Targeted next generation sequencing as a tool for precision medicine. BMC Med Genomics 12:81. https://doi.org/10.1186/s12920-019-0527-2
5. Asada K, Kaneko S, Takasawa K et al (2021) Integrated analysis of whole genome and epigenome data using machine learning technology: toward the establishment of precision oncology. Front Oncol 11:666937. https://doi.org/10.3389/fonc.2021.666937
6. Souza GR, Molina JR, Raphael RM et al (2010) Three-dimensional tissue culture based on magnetic cell levitation. Nat Nanotechnol 5(4):291–296. https://doi.org/10.1038/nnano.2010.23
7. Boughey JC, Suman VJ, Yu J et al (2021) Patient-derived xenograft engraftment and breast cancer outcomes in a prospective neoadjuvant study (beauty). Clin Cancer Res 27(17):4696–4699. https://doi.org/10.1158/1078-0432.Ccr-21-0641
8. Li M, Belmonte JCI (2019) Organoids—preclinical models of human disease. New Engl J Med 380(6):569–579. https://doi.org/10.1056/NEJMra1806175
9. Method of the year 2017: organoids. Nat Methods 15(1):1. https://doi.org/10.1038/nmeth.4575
10. Koh V, Chakrabarti J, Torvund M et al (2021) Hedgehog transcriptional effector GLI mediates mTOR-induced PD-L1 expression in gastric cancer organoids. Cancer Lett 518:59–71. https://doi.org/10.1016/j.canlet.2021.06.007
11. Bose S, Clevers H, Shen X (2021) Promises and challenges of organoid-guided precision medicine. Med 2(9):1011–1026. https://doi.org/10.1016/j.medj.2021.08.005
12. Borries M, Barooji YF, Yennek S et al (2020) Quantification of visco-elastic properties of a matrigel for organoid development as a function of polymer concentration. Front Phys 8:579168. https://doi.org/10.3389/fphy.2020.579168
13. Gao D, Vela I, Sboner A et al (2014) Organoid cultures derived from patients with advanced prostate cancer. Cell 159(1):176–187. https://doi.org/10.1016/j.cell.2014.08.016
14. Vlachogiannis G, Hedayat S, Vatsiou A et al (2018) Patient-derived organoids model treatment response of metastatic gastrointestinal cancers. Science 359(6378):920–926. https://doi.org/10.1126/science.aao2774
15. Boehnke K, Iversen PW, Schumacher D et al (2016) Assay establishment and validation of a high-throughput screening platform for three-dimensional patient-derived colon cancer organoid cultures. J Biomol Screen 21(9):931–941. https://doi.org/10.1177/1087057116650965
16. Driehuis E, Kretzschmar K, Clevers H (2020) Establishment of patient-derived cancer organoids for drug-screening applications. Nat Protoc 15(10):3380–3409. https://doi.org/10.1038/s41596-020-0379-4
17. Geuens T, van Blitterswijk CA, LaPointe VLS (2020) Overcoming kidney organoid challenges for regenerative medicine. NPJ Regen Med 5(1):8. https://doi.org/10.1038/s41536-020-0093-4
18. Brandenberg N, Hoehnel S, Kuttler F et al (2020) High-throughput automated organoid culture via stem-cell aggregation in microcavity arrays. Nat Biomed Eng 4(9):863–874. https://doi.org/10.1038/s41551-020-0565-2
19. Hou Y, Ai XN, Zhao L et al (2020) An integrated biomimetic array chip for high-throughput co-culture of liver and tumor microtissues for advanced anticancer bioactivity screening. Lab Chip 20(14):2482–2494. https://doi.org/10.1039/d0lc00288g
20. Xiao RR, Lv T, Tu X et al (2021) An integrated biomimetic array chip for establishment of collagen-based 3D primary human hepatocyte model for prediction of clinical drug-induced liver injury. Biotechnol Bioeng 118(12):4687–4698. https://doi.org/10.1002/bit.27931
21. Park SE, Georgescu A, Huh D (2019) Organoids-on-a-chip. Science 364(6444):960–965. https://doi.org/10.1126/science.aaw7894
22. Wan L, Neumann CA, Leduc PR (2020) Tumor-on-a-chip for integrating a 3D tumor microenvironment: chemical and mechanical factors. Lab Chip 20(5):873–888. https://doi.org/10.1039/c9lc00550a
23. Wasson EM, Dubbin K, Moya ML (2021) Go with the flow: modeling unique biological flows in engineered in vitro platforms. Lab Chip 21(11):2095–2120. https://doi.org/10.1039/d1lc00014d
24. Ai XN, Zhao L, Lu YY et al (2020) Integrated array chip for high-throughput screening of species differences in metabolism. Anal Chem 92(17):11696–11704. https://doi.org/10.1021/acs.analchem.0c01590

25. Ai XN, Lu WB, Zeng KW et al (2018) Microfluidic coculture device for monitoring of inflammation induced myocardial injury dynamics. Anal Chem 90(7):4485–4494. https://doi.org/10.1021/acs.analchem.7b04833
26. Hu YW, Sui XZ, Song F et al (2021) Lung cancer organoids analyzed on microwell arrays predict drug responses of patients within a week. Nat Commun 12(1):2581. https://doi.org/10.1038/s41467-021-22676-1
27. Jiang SW, Zhao HR, Zhang WJ et al (2020) An automated organoid platform with inter-organoid homogeneity and inter-patient heterogeneity. Cell Rep Med 1(9):100161. https://doi.org/10.1016/j.xcrm.2020.100161
28. Rawal P, Tripathi DM, Ramakrishna S et al (2021) Prospects for 3D bioprinting of organoids. Bio-Des Manuf 4(3):627–640. https://doi.org/10.1007/s42242-020-00124-1
29. Van Zundert I, Fortuni B, Rocha S (2020) From 2D to 3D cancer cell models—the enigmas of drug delivery research. Nanomaterials 10(11):2236. https://doi.org/10.3390/nano10112236
30. Wilson SS, Mayo M, Melim T et al (2021) Optimized culture conditions for improved growth and functional differentiation of mouse and human colon organoids. Front Immunol 11:547102. https://doi.org/10.3389/fimmu.2020.547102
31. Grabinger T, Luks L, Kostadinova F et al (2014) Ex vivo culture of intestinal crypt organoids as a model system for assessing cell death induction in intestinal epithelial cells and enteropathy. Cell Death Dis 5(5):e1228. https://doi.org/10.1038/cddis.2014.183
32. Agarwal T, Celikkin N, Costantini M et al (2021) Recent advances in chemically defined and tunable hydrogel platforms for organoid culture. Bio-Des Manuf 4(3):641–674. https://doi.org/10.1007/s42242-021-00126-7
33. Choi JI, Jang SI, Hong J et al (2021) Cancer-initiating cells in human pancreatic cancer organoids are maintained by interactions with endothelial cells. Cancer Lett 498:42–53. https://doi.org/10.1016/j.canlet.2020.10.012
34. Takigawa H, Kitadai Y, Shinagawa K et al (2016) Multikinase inhibitor regorafenib inhibits the growth and metastasis of colon cancer with abundant stroma. Cancer Sci 107(5):601–608. https://doi.org/10.1111/cas.12907
35. Backes Y, Seerden TCJ, Van Gestel RSFE et al (2019) Tumor seeding during colonoscopy as a possible cause for metachronous colorectal cancer. Gastroenterology 157(5):1222–1232. https://doi.org/10.1053/j.gastro.2019.07.062
36. Heydari Z, Moeinvaziri F, Agarwal T et al (2021) Organoids: a novel modality in disease modeling. Bio-Des Manuf 4(4):689–716. https://doi.org/10.1007/s42242-021-00150-7
37. Lau HCH, Kranenburg O, Xiao HP et al (2020) Organoid models of gastrointestinal cancers in basic and translational research. Nat Rev Gastro Hepat 17(4):203–222. https://doi.org/10.1038/s41575-019-0255-2
38. Skala MC, Deming DA, Kratz JD (2022) Technologies to assess drug response and heterogeneity in patient-derived cancer organoids. Annu Rev Biomed Eng 24:157–177. https://doi.org/10.1146/annurev-bioeng-110220-123503
39. Sato T, Vries RG, Snippert HJ et al (2009) Single Lgr5 stem cells build crypt-villus structures in vitro without a mesenchymal niche. Nature 459(7244):262–265. https://doi.org/10.1038/nature07935
40. Kozlowski MT, Crook CJ, Ku HT (2021) Towards organoid culture without matrigel. Commun Biol 4(1):1387. https://doi.org/10.1038/s42003-021-02910-8
41. Jee JH, Lee DH, Ko J et al (2019) Development of collagen-based 3D matrix for gastrointestinal tract-derived organoid culture. Stem Cells Int 2019:8472712. https://doi.org/10.1155/2019/8472712
42. Sun Q, Zhou J, Zhang Z et al (2014) Discovery of fruquintinib, a potent and highly selective small molecule inhibitor of VEGFR 1, 2, 3 tyrosine kinases for cancer therapy. Cancer Biol Ther 15(12):1635–1645. https://doi.org/10.4161/15384047.2014.964087
43. Ding S, Hsu C, Wang Z et al (2022) Patient-derived micro-organospheres enable clinical precision oncology. Cell Stem Cell 29(6):905–917. https://doi.org/10.1016/j.stem.2022.04.006
44. Bose S, Clevers H, Shen XL (2021) Promises and challenges of organoid-guided precision medicine. Med-Cambridge 2(9):1011–1026. https://doi.org/10.1016/j.medj.2021.08.005
45. Van De Wetering M, Francies HE, Francis JM et al (2015) Prospective derivation of a living organoid biobank of colorectal cancer patients. Cell 161(4):933–945. https://doi.org/10.1016/j.cell.2015.03.053